CrossMark

# Variable Stars in the Giant Satellite Galaxy Antlia 2

A. Katherina Vivas[1] , Clara E. Martínez-Vázquez[1,2] , Alistair R. Walker[1] , Vasily Belokurov[3] , Ting S. Li[4] , and
Denis Erkal[5]

[1] Cerro Tololo Inter-American Observatory/NSF's NOIRLab, Casilla 603, La Serena, Chile
[2] Gemini Observatory/NSF's NOIRLab, 670 N. A'ohoku Place, Hilo, HI 96720, USA
[3] Institute of Astronomy, University of Cambridge, Madingley Road, Cambridge CB3 0HA, UK
[4] Department of Astronomy and Astrophysics, University of Toronto, 50 St. George Street, Toronto ON, M5S 3H4, Canada
[5] Department of Physics, University of Surrey, Guildford GU2 7XH, UK

## Abstract

We report 350 pulsating variable stars found in four DECam fields ($\sim$12 deg$^2$) covering the Antlia 2 satellite galaxy. The sample of variables includes 318 RR Lyrae stars and eight anomalous Cepheids in the galaxy. Reclassification of several objects designated previously to be RR Lyrae as anomalous Cepheids get rid of the satellite's stars intervening along the line of sight. This in turn removes the need for prolific tidal disruption of the dwarf, in agreement with the recently updated proper motion and pericenter measurements based on Gaia EDR3. There are also several bright foreground RR Lyrae stars in the field, and two distant background variables located $\sim$45 kpc behind Antlia 2. We found RR Lyrae stars over the full search area, suggesting that the galaxy is very large and likely extends beyond our observed area. The mean period of the RR$ab$ in Antlia 2 is 0.599 days, while the RR$c$ have a mean period of 0.368 days, indicating the galaxy is an Oosterhoff-intermediate system. The distance to Antlia 2 based on the RR Lyrae stars is 124.1 kpc ($\mu_0 = 20.47$) with a dispersion of 5.4 kpc. We measured a clear distance gradient along the semimajor axis of the galaxy, with the southeast side of Antlia 2 being $\sim$13 kpc farther away from the northwest side. This elongation along the line of sight is likely due to the ongoing tidal disruption of Ant 2.

*Unified Astronomy Thesaurus concepts:* RR Lyrae variable stars (1410); Dwarf galaxies (416); Local Group (929); Anomalous Cepheid variable stars (2106)

*Supporting material:* figure set, machine-readable tables

## 1. Introduction

The environment of the Milky Way (MW) contains more than 50 known smaller galaxies, that range in size from large dwarf galaxies such as the Magellanic Clouds with active star formation and absolute magnitude $M_V \sim -18$, to the many quiescent ultra faint dwarf (UFD) galaxies with luminosities similar to globular clusters (Simon 2019), the faintest of which have $M_V \sim 0$. Discovered mostly by deep wide-field imaging surveys in the past two decades (see reviews by Willman 2010; McConnachie 2012; Belokurov 2013; Simon 2019) many of these low stellar mass galaxies show signs of their interaction with the MW by elongated shape or by associated tidal debris. The plethora of stellar streams that are now known (see, e.g., Shipp et al. 2018) indicates that disruption events may be common. Analyses of the structure of our galaxy, together with chemo-dynamic analyses of the stellar content of the thick disk and halo, show that encounters and mergers have had a substantial effect on the properties of the MW over its lifetime, and are continuing to do so.

A convenient way to view the totality of the MW companion galaxies is by the size–luminosity plot (see, e.g., Figure 11 in Torrealba et al. 2019), which is well populated over 18 magnitudes in luminosity and half-light radii ($r_h$) from 20 to $\sim$4000 pc. However, the completeness as a function of position in this diagram is not well known except for the brighter

systems. Apart from galaxies hidden behind the Galactic plane, there is possible confusion between low luminosity globular clusters and the fainter UFDs, with the compilation of the fainter galaxies also likely to be severely incomplete. Future surveys such as the Vera C. Rubin Legacy Survey of Space and Time are expected to help redress this situation. Figure 1 shows a zoom of the size–luminosity plot in the region of the brightest and largest of the satellite galaxies. The low luminosity/large size region in Figure 1 appears uninhabited, but this could be an observational effect as such low surface brightness galaxies will be dominated by Galactic foreground stars. Indeed, the discovery of Crater 2 by Torrealba et al. (2016), and in particular, the subsequent discovery of Antlia 2 (Ant 2) by Torrealba et al. (2019) from Gaia proper motions in a field with much higher foreground contamination than Crater 2, shows how nearly invisible such objects can be.[6]

The RR Lyrae variable stars are a powerful tool for studying the morphology, metallicity, and age of, in particular, low surface brightness galaxies (Catelan & Smith 2015). Ubiquitous in any population more than $\sim$10 Gyr old (Savino et al. 2020), they are easy to identify even in very crowded fields, and being standard candles they can be definitively assigned (or not) to a minority population galaxy immersed in the MW. Apart from the rare case of Leo T (Clementini et al. 2012), all other UFD galaxies so far known terminated their star formation early ($\sim$10 Gyr or older; Simon 2019) and so the RR Lyrae stars are representative of the dominant (or only)

---

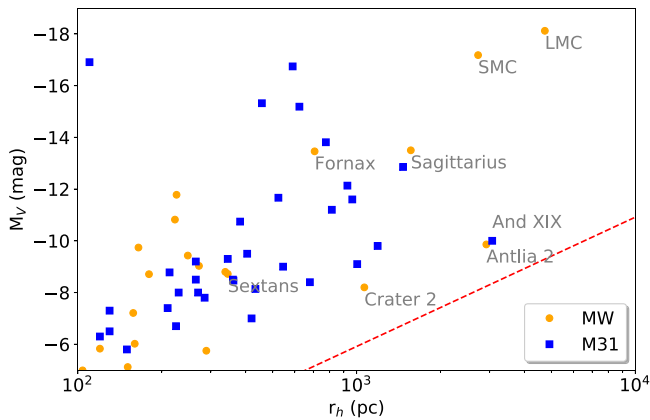[6] These galaxies can also be found under the names Antlia II and Crater II in the literature.

**Figure 1.** Absolute magnitude vs. half-light radius for satellite galaxies of the MW and M31 (McConnachie 2012; Martin et al. 2016; Drlica-Wagner et al. 2020; Ji et al. 2021). This plot zooms into the region of the brightest and largest satellite galaxies, with most UFDs lying outside the plotted region. The red dotted line indicates surface brightness $\mu = 32$ mag arcsec$^{-2}$.

**Table 1**
Log of the DECam Ant 2 Observations

| Run Date | $r, i$ Exposures | Image Quality (arcsec) | Comments |
|---|---|---|---|
| 2018 Nov 23 | 32 | 0.8 | Clear |
| 2018 Dec 19 | 56 | 1.0 | Clear |
| 2019 Jan 20 | 71 | 1.0 | Thin cirrus |
| 2019 Jan 21 | 117 | 1.0 | Thin cirrus |

**Table 2**
Central Coordinates of Observed Fields

| Field | $\alpha$ (J2000.0) (deg) | $\delta$ (J2000.0) (deg) |
|---|---|---|
| A | 143.08400 | −35.32892 |
| B | 144.81242 | −36.43172 |
| C | 142.87454 | −37.10664 |
| D | 144.81225 | −38.25325 |

population present in these galaxies. These properties of RR Lyrae stars are particularly useful when studying galaxies like Ant 2, which, being both a low surface brightness object and located at a galactic latitude of $b \sim +11°$, suffers from a very high foreground contamination.

The discovery of Ant 2 by Torrealba et al. (2019) was triggered by the identification of a group of three RR Lyrae stars in the Gaia DR2 catalog (Clementini et al. 2019), which were close together in the sky, shared similar proper motions, and were located at roughly the same distance. Further investigation by the discovery team, however, concluded that the RR Lyrae stars were not actually part of Ant 2 since they were located in front of it. Torrealba et al. (2019) suggested that those three RR Lyrae stars were the near side of a cloud of debris material originated from Ant 2 during its disruption by the tidal forces of the MW. A complete survey of RR Lyrae stars in this galaxy is needed to confirm/deny such a scenario.

In this paper we describe the search and discovery of RR Lyrae stars and other variables, either in Ant 2 or its line of sight, from observations made with the Dark Energy Camera (DECam; Flaugher et al. 2015), and discuss the properties of Ant 2 from an analysis of their pulsational properties and distribution. In Section 2, we describe the observations, data reduction and time series analysis. The population of RR Lyrae stars in Ant 2 is discussed in detail in Section 3, and we compare their spatial distribution with a model of the tidal disruption of Ant 2 in Section 4. Anomalous Cepheids (AC) in Ant 2 are described in Section 5. Finally, our conclusions are presented in Section 6, with time series data tabulated in the Appendix.

## 2. Observations

The Ant 2 observations presented here were collected using DECam on the Víctor M. Blanco 4 m telescope at the Cerro Tololo Inter-American Observatory, Chile, on two part nights in 2018 November and December, and two full nights in 2019 January, as detailed in Table 1. All these nights were close to full Moon, therefore we decided to observe in the $r$ and $i$ filters, with exposures of 180 and 240 s, respectively. With its 3 deg$^2$ field of view (FoV), DECam is an ideal instrument to study this large galaxy ($r_h = 1°27$; Torrealba et al. 2019). We used four pointings (Table 2), almost nonoverlapping, to cover the galaxy

(see Figure 2). During photometric conditions standard star fields were also observed.

The observational strategy consisted of imaging consecutively the four fields in $r$ and $i$, and then repeating the sequence but with an offset of 75″ and 60″ in $\alpha$ and $\delta$, respectively, to fill in the gaps between CCDs. During a night the typical time between observations of the same field/filter was ∼30 minutes.

### 2.1. Data Reduction and Photometry

The images were processed by the DECam Community Pipeline (Valdes & Gruendl 2014), which removes the instrument signature and provides several data products.[7] This was followed by application of the PHOTRED package as described in detail by Nidever et al. (2017). PHOTRED efficiently runs the DAOPHOT photometry programs (Stetson 1987, 1994) automatically on a night-by-night basis, after choosing options via a setup file. For the individual images, photometry was performed using the ALLSTAR program. Astrometry is referenced to the system of the Gaia catalog. We also ran a separate processing where all four nights were grouped together and the forced photometry program ALLFRAME used to produce a single photometry list for each pointing.

Photometric calibration was obtained from the standard star fields observed during clear conditions. The resulting photometry is on the Sloan Digital Sky Survey (SDSS) system. The left color–magnitude diagram (CMD) shown in Figure 3 contains 1,036,351 objects after isolating point sources by requiring the DAOPHOT morphological parameters to be chi $\leqslant 3.0$, $-1.0 \leqslant$ SHARP $\leqslant 1.0$, and PROB $\geqslant 0.8$. There are no clear features of the Ant 2 system in this CMD except by a horizontal branch (HB) at $r \sim 21$. The CMD is dominated by foreground populations, which at these low galactic latitudes ($b \sim 11°$) is large. The HB looks extended in brightness, which is a likely consequence of both differential extinction and distance gradient within the galaxy, as we discuss later in this paper (see Section 3.3). There is a hint of a blue plume population at $(r - i) < 0$ and $18 < r < 23.5$. Just from the CMD it is not obvious if this blue plume is evidence of a younger population present in Ant 2, or if it is formed by Galactic
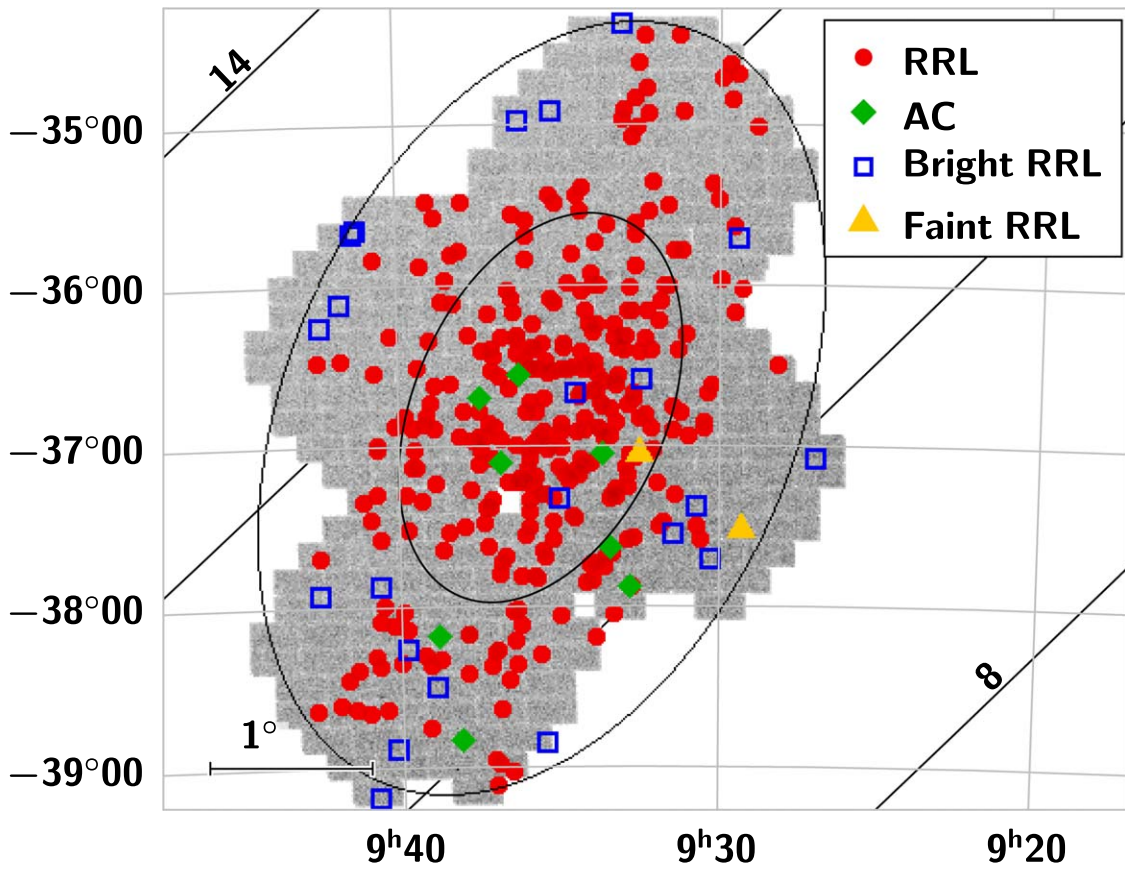
---

**Figure 2.** Spatial coverage of our DECam observations of Ant 2 in equatorial coordinates. The gray background, which shows the footprint of our survey, is a density map made with all stars in our catalog. The two black ellipses indicate the 1 $r_h$ and 2 $r_h$, as measured by Torrealba et al. (2019). Colored symbols indicate the location of pulsating variable stars found in the field: red circles and green diamonds are RR Lyrae stars and AC in Ant 2, while open blue squares indicate the location of bright RR Lyrae stars which are presumably field halo stars. The two yellow triangles show two faint RR Lyrae stars located beyond Ant 2. For reference the diagonal lines indicate lines of constant galactic latitude.
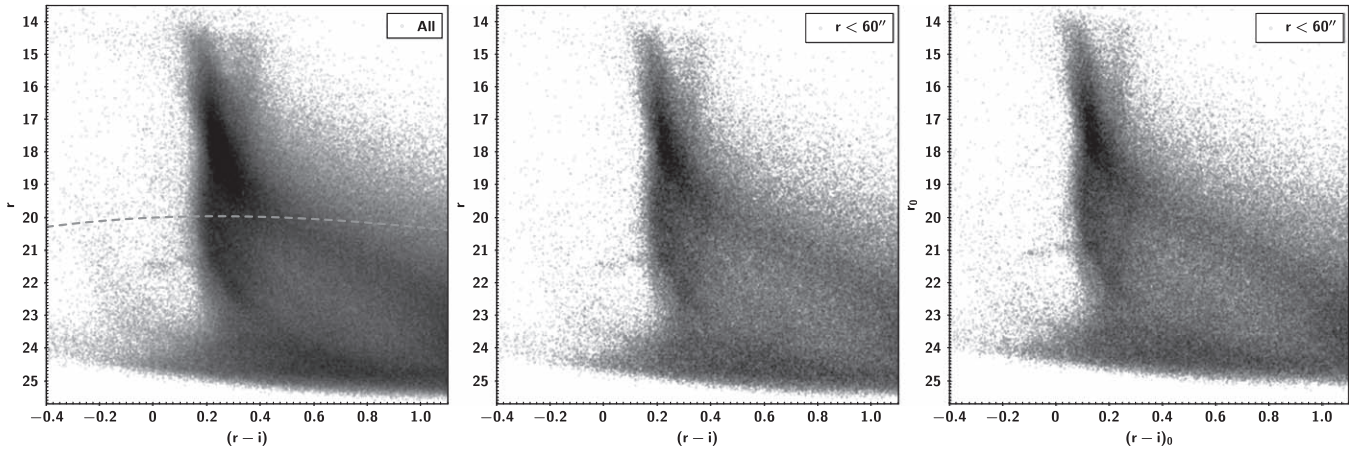


**Figure 3.** Left: observational CMD of the full observed area in Ant 2, containing $\sim 10^6$ stars. The gray dashed line indicates the Gaia limit ($G = 20$) we used to explore the blue plume population seen at $(r - i) \sim -0.2$. Middle: observational CMD showing only stars within 1° from the center of Ant 2, 297,064 stars. Right: reddening-corrected CMD of stars within 1° from the center of Ant 2.

foreground stars. To explore this, we analyzed parallaxes by Gaia EDR3 (Gaia Collaboration et al. 2021) for stars brighter than $G = 20$, shown in Figure 3 (left panel) as stars above the gray dashed line. The blue population only shows up for a high parallax selection, and the resulting absolute magnitudes suggest these blue stars are mostly white dwarfs and probably some more exotic objects like extreme horizontal branch stars or extremely low mass white dwarfs, which are significantly brighter than

normal white dwarfs. Although this quick analysis is limited only to the bright part of the CMD, the coherence of the observed feature suggest all of them are MW white dwarfs, which is not surprising since the line of sight to Ant 2 goes through the Galactic disk. This conclusion does not preclude Ant 2 from having some young main-sequence or blue straggler stars, but if these do indeed exist, they are likely few and hard to pick from the CMD.

The HB looks more defined and narrow when looking only at stars within a radius of $r < 1°$ (Figure 3, middle panel), where the extinction is more uniform and the distance gradient is less noticeable. Only when the CMD is corrected by extinction, a clear red giant branch (RGB) and HB is visible (Figure 3, right panel). We obtained $E(B - V)$ from the Schlegel et al. (1998) interstellar dust maps using the Python task dustmaps (Green 2018). The photometry is not deep enough to reach to the main-sequence turnoff of Ant 2.

### 2.1.1. Variable Stars

We selected variable stars from our catalog following the same recipe as in previous works by our group, namely, Vivas et al. (2016, 2019, 2020). In particular for this work, we preselected stars that were flagged as variables in both the $r$ and $i$ bands, have at least 12 observations in each band, have magnitudes in the range of $17 < r < 22.5$, colors in the range of $-0.3 < (r - i) < 0.4$, and an amplitude in the $r$ band of at least 0.1 mag. Then, the preselected stars were searched for periodicity in the range of 0.1–2.5 days, with the final selection and classification made by visual inspection of the phased light curves. These constraints were designed to find RR Lyrae and AC in the region of the instability strip, with a very loose color constraint to give room for variables with high reddening. The light curves we examined have an average of 33 epochs in each filter; in the region of overlap between fields there are light curves with as many as 68 epochs/filter.

We discovered numerous eclipsing binaries, a consequence of the large disk foreground population in our data, which are not studied further in this paper. Stars identified as first-overtone RR Lyrae pulsators, or RRc stars, which are prone to be contaminated by eclipsing binaries of the W Ursa Major type (e.g., Kinman & Brown 2010) because of their near to sinusoidal light curves, were carefully examined by looking at their colors and their location in a period–amplitude diagram. Several candidates were discarded as RRc because either they were too red for being this type of pulsator or because their amplitudes and periods did not lie in the correct locus of a Bailey (period versus amplitude) diagram.

In total we found 350 periodic variable stars in the Ant 2 field, which were preliminarily classified as RRab (211 stars), RRc (115 stars), RRd (21 stars), and AC (three stars). In the latter group the periods were too long ($>1$ day) to be classified as RR Lyrae. By placing the variable stars in the CMD (Figure 4), it seems clear that all the variables in the range of $19.5 < r < 20.8$ should be AC stars in Ant 2. In this group there are eight stars, including the three variables with longer periods mentioned before as well as five stars classified initially as RRab and RRc. So after reclassifying these as AC stars, the final numbers are 342 RR Lyrae stars (207 RRab, 114 RRc, and 21 RRc), and eight AC. Table 3 lists the properties of all the stars: ID, R.A., decl., pulsational period, number of observations, amplitude and mean magnitude in each band ($r$ and $i$), extinction in $i$, and type of variable. The ID numbering from V1–V350 was assigned according to the elliptical distance (see Section 3.4) with the lower numbers being those closer to the center of Ant 2. Amplitudes and mean magnitudes for RRab and RRc were obtained from the best-fitted template (from the library by Sesar et al. 2010) to the light curves. The mean magnitudes were obtained by integrating the templates in intensity units and transforming the result back to magnitudes.

As shown in Figure 4 and in a histogram of magnitudes of the variable stars (Figure 5), there is a group of 22 bright RR
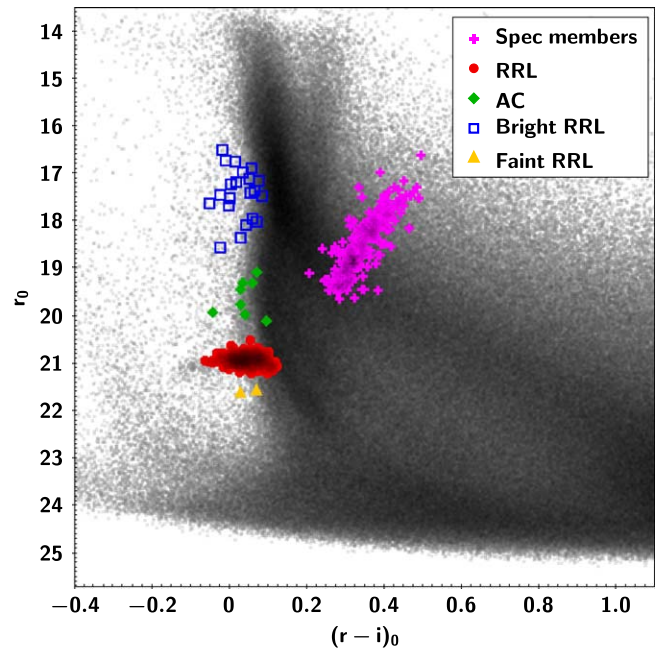


**Figure 4.** Reddening-corrected CMD with the variable stars identified in this work. For reference, we also show the high probability spectroscopic members in the RGB of Ant 2, as identified by Ji et al. (2021).

Lyrae stars with $r < 19.0$ that are classified as a foreground population from the halo, and possibly alternatively from the thick disk, of the MW. These bright RR Lyrae stars are located at distances between 16 and 40 kpc from the Sun. The majority of the RR Lyrae stars in our sample (318 stars, 91%), however, are concentrated in the HB of Ant 2 at $r \sim 21.3$ in the CMD. We discuss these stars in detail in the next section. In addition, there are two RR Lyrae stars (V134 and V304) that lie well below the HB ($r > 21.9$), and thus appear to be located behind Ant 2 (see Section 3.3.1 for further discussion).

A sample of light curves is shown in Figure 6, including two bright (foreground) RR Lyrae stars, two AC, six RR Lyrae stars in Ant 2 (two of each type), and finally the two faint RR Lyrae stars likely located behind Ant 2. The full photometry data set and light curves for all the variables can be found in the Appendix. For the RR Lyrae stars in Ant 2, the typical photometric errors of the individual epochs are 0.04 and 0.03 mag in $r$ and $i$, respectively

Most of the periodic variable stars found in this work are new discoveries since they are fainter than the limiting magnitude for most wide surveys of variables such as the CRTS (Drake et al. 2014) or Gaia (Clementini et al. 2019). We matched our catalog with the Gaia DR2 RR Lyrae star listing (Clementini et al. 2019) and found 17 stars in common, all of them brighter than $r < 20.3$. The RR Lyrae stars in Ant 2 are just too faint for Gaia. On the other hand, there are 39 Gaia RR Lyrae stars within our footprint, and we did not recover 21 of them, mostly because they were too bright ($r < 17$) for our survey. There are, however, two Gaia RR Lyrae stars in the range $18.5 < r < 20.2$ that are in our magnitude range; they were indeed flagged as variable but we were unable to find a period for them.[8] In one case the star was located close to the border of one field and had only $\sim15$ epochs/band, which was not enough to obtain a period, although our data is consistent

---

8  Gaia IDs are 5437028340146753664 and 5436057883696115328.

**Table 3**
Periodic Variable Stars in the Field of Ant 2

| ID | α (deg) | δ (deg) | Period (days) | N (r) | Amp (r) (mag) | Mean r (mag) | N (i) | Amp (i) (mag) | Mean i (mag) | $A_i$ (mag) | Dist (kpc) | σDist (kpc) | Type[a] |
|----|---------|---------|---------------|-------|---------------|--------------|-------|---------------|--------------|-------------|------------|-------------|---------|
| V1 | 143.87486 | −36.91461 | 0.66093 | 41 | 0.61 | 21.29 | 41 | 0.38 | 21.16 | 0.27 | 129.4 | 2.6 | ab |
| V2 | 143.73833 | −36.86352 | 0.35250 | 65 | 0.66 | 21.10 | 67 | 0.41 | 20.98 | 0.26 | ⋯ | ⋯ | c |
| V3 | 143.90192 | −36.93597 | 0.39555 | 46 | 0.52 | 21.33 | 46 | 0.25 | 21.18 | 0.27 | 124.2 | 2.5 | c |
| V4 | 143.73605 | −36.91526 | 0.56934 | 26 | 0.88 | 21.31 | 25 | 0.66 | 21.19 | 0.26 | 127.2 | 2.5 | ab |
| V5 | 143.93247 | −36.79384 | 0.39872 | 67 | 0.49 | 21.37 | 66 | 0.30 | 21.25 | 0.26 | 129.2 | 2.6 | c |
| V6 | 143.94381 | −36.98518 | 0.60702 | 33 | 0.28 | 21.36 | 34 | 0.21 | 21.19 | 0.28 | 128.4 | 2.6 | ab |
| V7 | 143.83054 | −36.99803 | 0.58207 | 34 | 0.63 | 21.34 | 33 | 0.52 | 21.19 | 0.28 | 127.1 | 2.5 | ab |
| V8 | 143.83305 | −37.02513 | 0.37702 | 34 | 0.49 | 21.40 | 29 | 0.30 | 21.24 | 0.28 | 126.2 | 2.5 | c |

**Note.**
[a] Types: ab = type ab RR Lyrae stars; c = type c RR Lyrae stars; AC = anomalous Cepheids; Fab = type ab field RR Lyrae stars; Fc = type c field RR Lyrae stars;
(This table is available in its entirety in machine-readable form.)
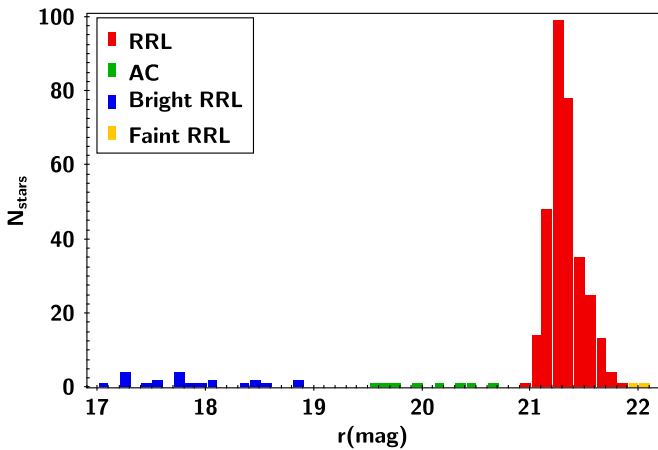


**Figure 5.** Histogram of the mean r magnitudes of all periodic variable stars found in the field of Ant 2.

with the Gaia period. In the second case, the Gaia star has $G = 20.2$, which is close to the faint limit for the RR Lyrae stars in that catalog. Our data does not agree either with the period nor with the amplitude given by Gaia, hinting for a possible misclassification.

## 3. RR Lyrae Stars in Ant 2

There are 318 RR Lyrae stars in Ant 2 of which 193 are RRab, 104 are RRc, and 21 are double mode pulsators, or RRd. We discuss their properties in the following subsections.

### 3.1. Oosterhoff Type

The Oosterhoff type (Oo; Oosterhoff 1939) was originally applied to RR Lyrae in galactic globular clusters; it revealed a dichotomy in the mean periods and in the ratio of the numbers of fundamental (RRab) and first-overtone (RRc) variables. This dichotomy is not observed in most of the satellite galaxies of the MW (Catelan 2009) and M31 (Martínez-Vázquez et al. 2017), which are usually classified as Oosterhoff-intermediate (Oo-int) since their properties lie in between those for the two original Oo I and Oo II groups.

The mean period of the RRab in Ant 2 is 0.599 days, while the RRc have a mean period of 0.368 days. The ratio $N_c/(N_{ab} + N_c)$ is 0.35. From Smith (1995), mean periods of RRab are 0.55d and 0.64d, and mean periods of RRc are 0.32d and 0.37 days for Oo I and Oo II systems, respectively. From the same source, the ratio

of type c stars over the sum of ab and c are 0.17 and 0.44 for Oo I and Oo II, respectively. Comparing these values with our data, Ant 2 is clearly in the middle between the two Oo groups, suggesting a Oo-int classification the same as found for many other dSph galaxies in the MW neighborhood.

A Bailey diagram, a plot of amplitude of the light curve versus period, is now considered (Smith 1995) the best way to infer the Oo classification of a stellar system. In Figure 7 we show the Bailey diagram for Ant 2, and the fiducial lines for Oo I and Oo II as defined by Fabrizio et al. (2019) but scaled by a factor of 0.94 to take into account that we have amplitudes in the r band and not in V. The scale factor was calculated by comparing the amplitudes of RR Lyrae stars in common between SDSS Stripe 82 (Sesar et al. 2010) and CRTS (Drake et al. 2014). The RRab stars in Ant 2 are mostly found between the fiducial lines for the Oo I and Oo II group, confirming that Oo-int is indeed the best classification for this system.

We estimate the percentage of Oo I and Oo II *like* stars in Ant 2 by counting how many RRab stars are located on each side of the Oo-int relation by Fabrizio et al. (2019). We obtained that 75% of the stars are Oo I while 25% are Oo II *like*. These results are consistent with what was found in Martínez-Vázquez et al. (2017) for RR Lyrae stars in Local Group dwarf galaxies where the majority of stars (∼80%) are distributed close to the locus of Oo I type.

### 3.2. Spatial Distribution

The on-sky spatial distribution of the RR Lyrae stars in Ant 2 can be seen in Figure 2. RR Lyrae stars were found in the full footprint of our observations, which reaches ∼$2r_h$. Although the density of stars clearly decreases with distance from the center of the galaxy, it is very likely that there are additional stars extending beyond $2r_h$.

Because of the very low surface brightness of Ant 2, combined with its low galactic latitude, contamination by fore/background stars is a challenge when analyzing the properties of the galaxy. By contrast, the RR Lyrae stars are a very pure sample of members of the galaxy. There is virtually no contamination by halo stars at this large distance from the Galactic center. Thus, we used the RR Lyrae stars to infer the shape of Ant 2 by fitting a bivariate Gaussian distribution[9] to the RR Lyrae stars to find the center, ellipticity ($\epsilon$), position angle (PA) and size of Ant 2. The results can be seen in

---

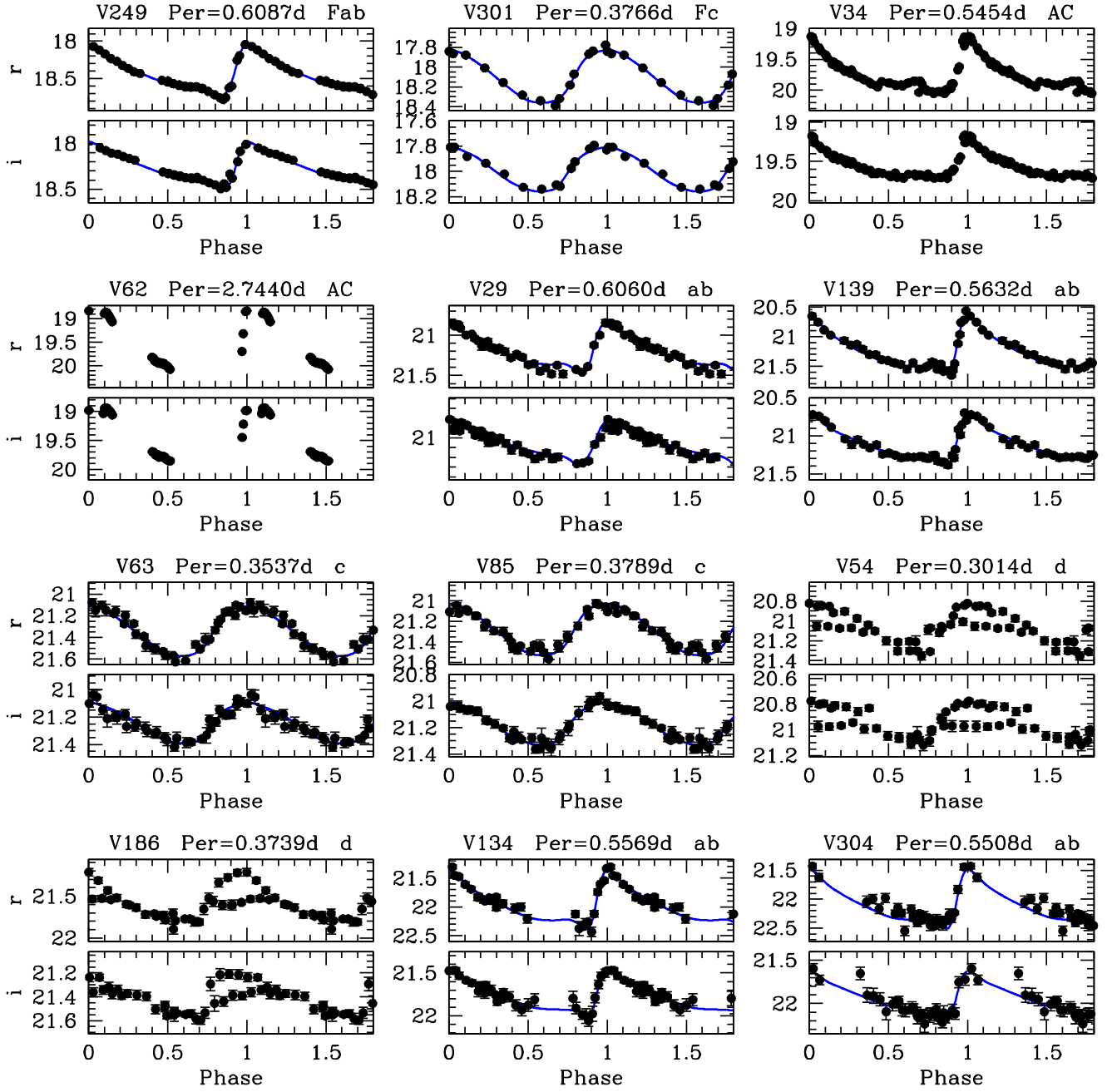[9] Using AstroML fit-bivariate_normal routine (Ivezić et al. 2014).

**Figure 6.** Sample of light curves. For each star the $r$, $i$ data are displayed in the top/bottom panels. Stars V249 and V301 are bright (foreground) RR Lyrae stars; V34 and V62 are AC; V29 and V139 are RRab in Ant 2; V63 and V85 are RR$c$ in Ant 2; V54 and V186 are RR$d$ in Ant 2, phased with their first overtone periods; V134 and V304 are the two faint RR Lyrae stars in the background of Ant 2. For all the types $ab$ and $c$ the underlying blue line is the best-fitted template to the light curve.

Figure 8, and in Table 4. Within the $1\sigma$ errors, we found the same center and ellipticity as Torrealba et al. (2019). The position angle is slightly different with respect to the one obtained Torrealba et al. (2019) but within $2\sigma$ errors of each other. There is more disagreement with the structural parameters found by Ji et al. (2021), particularly in the ellipticity, since they find a significantly more elongated structure than us. We obtain a $1\sigma$ semimajor axis of $52'.6$. Since we fitted Gaussian distributions this value is not directly comparable with $r_h$ from either Torrealba et al. (2019) nor Ji et al. (2021). We note that this elongation is aligned with the reflex corrected proper motions, once the LMC is accounted for (see Ji et al. 2021, for more details).

### 3.3. Distance to Ant 2 and Distance Gradient

One of the most important characteristics of RR Lyrae stars is that they are very good standard candles. Here we use the large number of variables in Ant 2 to determine the distance to the galaxy. Extinction is high and variable in this part of the sky due to the low galactic latitude location of Ant 2 (Figure 9). We obtained extinctions from the Schlafly & Finkbeiner (2011)'s recalibration of the dust maps by Schlegel et al. (1998). The mean extinction of the RR Lyrae stars in Ant 2 in the $r$ band is $A_r = 0.41$ mag, but is as high as 0.76 mag for some stars. Figure 9 shows that there is a region of relatively low extinction corresponding approximately with the central region of the galaxy.
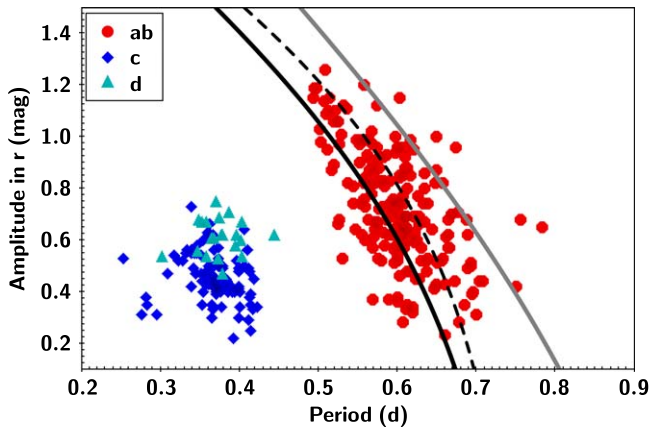
**Figure 7.** Bailey diagram of RR Lyrae stars in Ant 2. The black solid, gray solid, and black dashed lines represent the locus of Oo I, Oo II, and Oo-int systems, scaled to the $r$ band from Fabrizio et al. (2019).



**Figure 8.** Shape of the Ant 2 galaxy from fitting a bivariate Gaussian to the RR Lyrae star sample. In red we show the center and the $1\sigma$ and $3\sigma$ semimajor axis of the resulting ellipse. For comparison we also show the center (blue and green crosses) and shape parameters (blue and green ellipses) determined by (Torrealba et al. 2019, T19) and (Ji et al. 2021, J21). For those two cases the semimajor axis of the ellipse represents the half-light radius ($r_h$) of the galaxy.

The extinction increases toward the extremities of Ant 2, particularly toward the south.

After correcting magnitudes for interstellar extinction, we calculated the distance to each individual RR Lyrae star using the Period-Luminosity (PL) relation by Cáceres & Catelan (2008) in the $i$ band, which has a formal uncertainty of 0.045 mag. This relationship has a metallicity dependence for which we used the recent value of $[Fe/H] = -1.90$ (with a dispersion $\sigma = 0.34$) derived by Ji et al. (2021). The PL relation was applied to all RR$ab$ and RR$c$ stars (Table 5). For the later, we first fundamentalized the periods. We did not use RR$d$ stars because for these stars we did not fit a template to the light curves and hence do not have a mean magnitude measured in the same way as the other stars. The results from RR$ab$ and RR$c$ are consistent with each other (Table 5).

The mean distance given by the 297 RR Lyrae stars is 124.1 kpc, with a standard deviation of 5.4 kpc. The corresponding distance modulus is $\mu_0 = 20.47$ with a dispersion of 0.09 mag. The mean of the individual errors in Ant 2 is 2.5 kpc, and thus significantly lower than the standard deviation of the distribution. In order to ascertain what might be causing the large standard deviation in the distance distribution we first explored any spatial dependence of distance (Figure 9, bottom). It is clear from this map that there is a gradient of distance in Ant 2 with the southeast part of the galaxy being farther away than the northwest side. However, extinction is much higher to the southeast of Ant 2 (Figure 9, top) and may be influencing the distance determinations.

To better explore any possible correlation between the observed distance gradient and the extinction we transformed the equatorial coordinates $(\alpha, \delta)$ to planar coordinates $(\xi, \eta)$ with Ant 2 centered at (0, 0), and we rotated the system so the semimajor axis of the galaxy obtained here (Table 4) lies along the $x$-axis $(\xi')$. Figure 10 (top) shows the extinction as a function of the semimajor axis. In this coordinate system, the southeast part of Ant 2 is on the right side of the plot (positive $\xi'$). The middle panel shows the distance to the RR Lyrae stars as a function of the semimajor axis and the distance gradient suggested by the map in Figure 9 (bottom) is now clearer. The red line shows the best linear fit to the data, which has a slope of 2.66 kpc deg$^{-1}$ along the semimajor axis, and a distance at $\xi' = 0°$ of 124.2 kpc. Thus, in 5° from one side of the galaxy to the other, there is a difference in distance of ~13 kpc, which is much larger than the individual errors in distance.
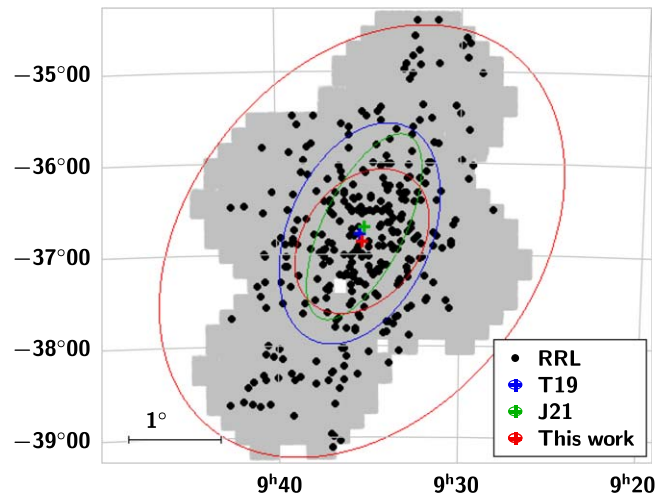
As seen in the upper panels of Figure 10, the behavior of both extinction and distance along the semimajor axis is completely different and thus the observed distance gradient is likely real rather than an effect of improper reddening correction. As a final check, we defined a "low-extinction" sample defined (arbitrarily) as all stars with $A_r < 0.46$ mag. The distance gradient is still visible in this reduced sample of 238 stars (Figure 10, bottom-left panel). The best-fitted line in this case has a slope of 2.72 kpc deg$^{-1}$ along the semimajor axis, and intersection with the $y$-axis at 124.1 kpc. These values are almost identical to the full sample and confirm that extinction is not causing the observed distance gradient. The gradient measured as a function of decl. is $-2.44$ kpc deg$^{-1}$ (full sample). We provide this alternative value since decl. is a fixed parameter and the semimajor axis depends instead on the assumed structural parameters of the galaxy.

The bottom-right panel in Figure 10 shows that the distance gradient observed in the RR Lyrae star population agrees quite well with the expectations from the disruption model of Ant 2 developed by Ji et al. (2021) and modified here to account for the mean distance given by the RR Lyrae stars which is slightly different to the value assumed in (Ji et al. 2021, 132 kpc). More discussion on the disruption model can be found below in Section 4.

### 3.3.1. RR Lyrae Stars Beyond Ant 2?

We return to the case of stars V134 and V304, the two RR$ab$ stars that lie below the HB of Ant 2, at mean $r$ magnitudes of 21.94 and 22.07, respectively. We showed their light curves in Figure 6. They are well sampled on both filters and they have small photometric errors, casting no doubt on their classification. Following the same procedure to calculate distances discussed in the previous section, we estimate that V134 is located at $167 \pm 4$ kpc and V304 is at $173 \pm 4$ kpc. Within $1\sigma$ errors, both stars are located at the same distance, but they are ~45 kpc behind Ant 2, which is a distance much larger than the distance errors or the distance dispersion of Ant 2.

**Table 4**
Shape Parameters of Ant 2

| | $\alpha$(J2000.0) (deg) | $\delta$ (J2000.0) (deg) | $\epsilon$ | PA (deg) | $1\sigma$ Semimajor Axis (deg) | $r_h$ (deg) |
|---|---|---|---|---|---|---|
| This work | $143.83 \pm 0.02$ | $-36.86 \pm 0.02$ | $0.28 \pm 0.03$ | $141 \pm 3$ | $0.88 \pm 0.03$ | |
| Torrealba et al. (2019) | $143.87 \pm 0.05$ | $-36.77 \pm 0.10$ | $0.38 \pm 0.08$ | $156 \pm 6$ | | $1.27 \pm 0.12$ |
| Ji et al. (2021) | $143.81 \pm 0.05$ | $-36.70 \pm 0.08$ | $0.60 \pm 0.04$ | $154 \pm 2$ | | $1.11 \pm 0.08$ |
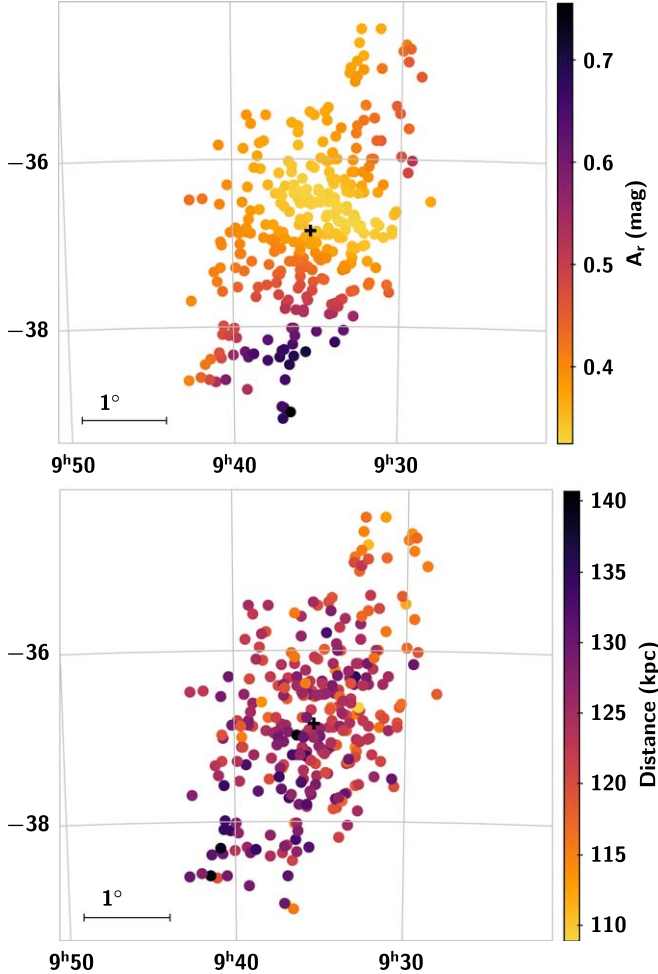


**Figure 9.** Top: map in equatorial coordinates of the interstellar extinction in the $r$ band for all the RR Lyrae stars found in Ant 2 from Schlafly & Finkbeiner (2011). Bottom: map of the individual distances to RR Lyrae stars (type $ab$ and $c$ only). In both plots, the black cross marks the center of the distribution of the RR Lyrae stars.

**Table 5**
Distance to Ant 2

| Type | Distance (kpc) | Std Dev (kpc) | $N$ |
|---|---|---|---|
| $ab$ | 124.7 | 5.5 | 193 |
| $c$ | 123.0 | 4.9 | 104 |
| All | 124.1 | 5.4 | 297 |

UFD galaxy. However, in principle they could be members of a stream. Models of the disruption of Ant 2 (see Section 4) do not support the presence of debris material behind the main body of the galaxy. At present then, we do not have a good explanation for the origin of these two very distant RR Lyrae stars.

### 3.4. Radial Profiles

The top panel of Figure 11 shows the profile of the number of RR Lyrae stars (only RR$ab$ and RR$c$) as a function of the elliptical distance ($r'$). This distance was obtained taking into account the center, ellipticity, and position angle of the galaxy as derived in this work (Table 4), and considering it as half the geometrical constant of the ellipse at the location of each individual RR Lyrae star. The radial profile was obtained using a running average, sorting the sample in distance, and counting the number of RR Lyrae stars within a fixed-size box of $15'$ and moving in steps of $5'$. The radial profile appears quite smooth, with just a slight overdensity near $100'$.

### 4. Comparison with a Model of the Tidal Disruption of Ant 2

Next, we compare our RR Lyrae star sample with models of the disruption of Ant 2. We use the same approach as in Ji et al. (2021), which simulated the tidal tails of Ant 2 in the presence of the MW and the Large Magellanic Cloud (LMC). These models use the modified Lagrange cloud stripping algorithm of Gibbons et al. (2014), which was generalized in Erkal et al. (2019) to include the effect of the LMC. This algorithm works by integrating the progenitor backward from the present-day location of Ant 2 for 5 Gyr in the presence of the MW and LMC. The system is then evolved forwards in time with particles ejected from the Lagrange points to generate the tidal debris around Ant 2. As in Ji et al. 2021, we model Ant 2 as a Plummer sphere with an initial mass of $10^{7.92} M_\odot$ and a scale radius of 1 kpc. The MW is modeled using the results of McMillan (2017). As in Ji et al. (2021), we use an MW model drawn from the posterior chains of McMillan (2017), which several works have shown is able to fit multiple streams in the MW (e.g., Li et al. 2021; Shipp et al. 2021)[10]. This MW has a mass of $8.27 \times 10^{11} M_\odot$ and gives a realistic past orbit of the LMC,

The stars are well within $2r_h$ of Ant 2, at $0\overset{\circ}{.}6$ and $1\overset{\circ}{.}4$ from the center of the galaxy, both of them to the southwest side of the field (Figure 2). They are separated by $47'$ from each other.

By integrating the number density radial profile of RR Lyrae from Medina et al. (2018) between 150 and 200 kpc, we estimate only 0.2 RR Lyrae stars are expected in that range of distances in an area of 12 deg$^2$ (our surveyed area). Thus, the possibility of having two random halo field stars this close in the sky, and at this distance is very low. These stars are either an indication of a separate stellar system behind Ant 2, or they may be part of material that have been torn apart from Ant 2 in the past. Since the stars are separated by $47'$ from each other, it is unlikely they belong to a compact stellar system such as a

---

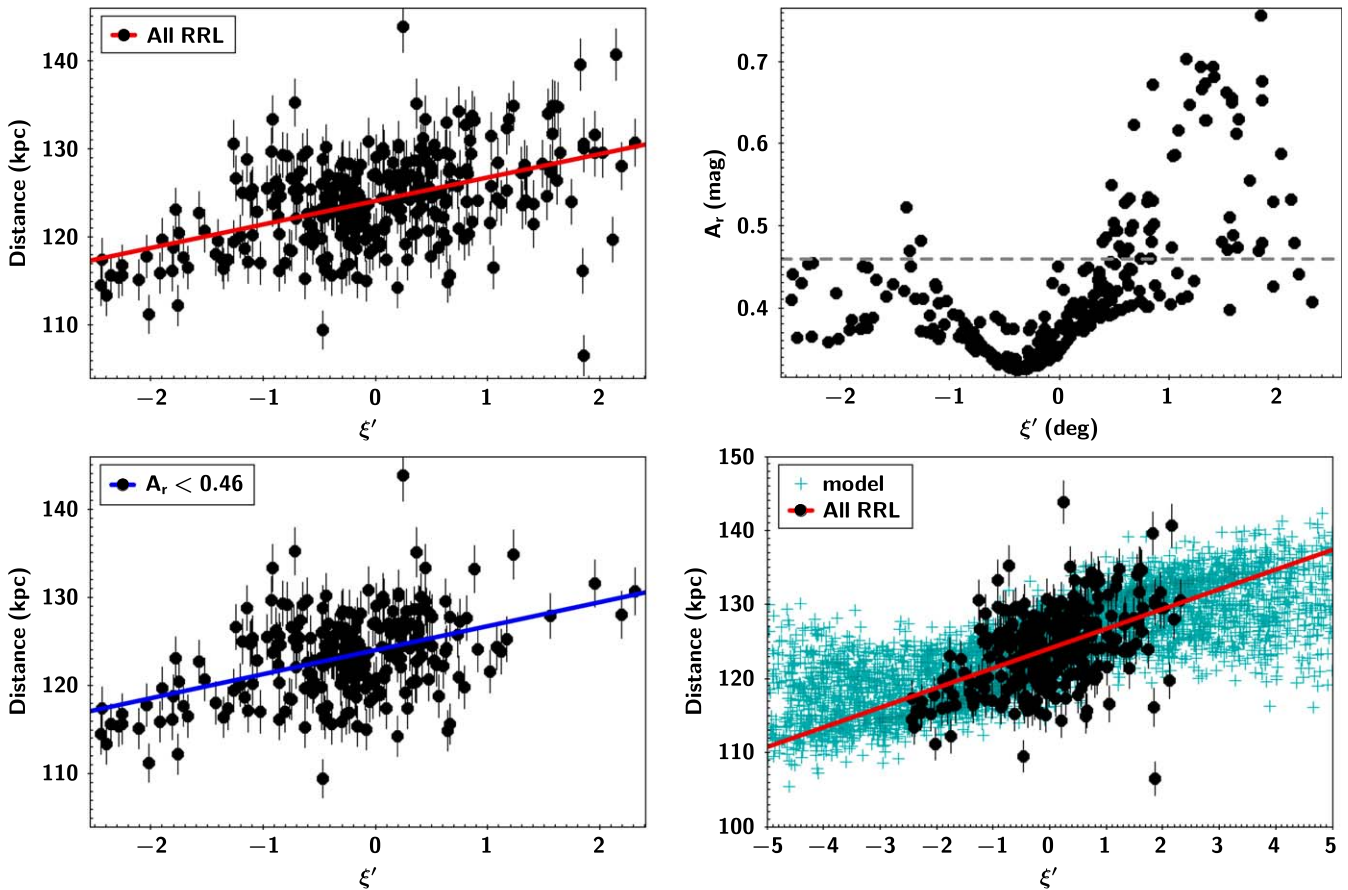[10] See Table A3 in Shipp et al. (2021) for the potential parameters.

**Figure 10.** Left: distance to the RR Lyrae stars along the semimajor axis of Ant 2. The red line is the best fit to the data. The bottom plot shows the same as above but for the RR Lyrae stars in the low-extinction sample. Right, top: interstellar extinction, $A_r$, of RR Lyrae stars along the semimajor axis of Ant 2. The dashed gray line at $A_r = 0.46$ is an arbitrary limit to define a low-extinction sample. Right, bottom: same as the left panels but with a wider view in both axis. The cyan crosses in the background represent the disruption model of Ant 2. The red line is the same as in the top-left panel.

consistent with it being on first approach to the MW (e.g., Besla et al. 2007). We evaluate the accelerations in this potential using galpot (Dehnen & Binney 1998). We model the LMC as a Hernquist profile with a mass of $1.5 \times 10^{11} M_\odot$ and a scale radius of 17.14 kpc motivated by the results of Erkal et al. (2019). We place the Sun at a Galactocentric distance of 8.122 kpc with a velocity of (11.1, 245.04, 7.25) km s$^{-1}$. For the LMC, we use a present-day proper motion, distance, and radial velocity from Kallivayalil et al. (2013), Pietrzyński et al. (2013), and van der Marel et al. (2002), respectively.

For Ant 2, we assume a distance of 124.1 kpc from Table 5, and use proper motions and radial velocities from Ji et al. (2021), $(\mu_\alpha^*, \mu_\delta) = (-0.094, 0.103)$ mas yr$^{-1}$ and $v_r = 288.8$ km s$^{-1}$, respectively. The resulting tidal debris is shown in Figure 12, alongside the RR Lyrae stars identified in this work. We note that the coordinates shown here are a top-down view of the present-day orbital plane of Ant 2. The red vector shows the present-day velocity vector of Ant 2 and the dashed-red curve shows the past orbit of Ant 2. The black points show the RR Lyrae stars, the blue points show the predicted tidal debris of Ant 2, and the orange points show the predicted debris within the on-sky footprint of the RR Lyrae star sample. This shows that within the orbital plane of Ant 2, the RR Lyrae stars are extended almost perpendicular to the present-day orbit of Ant 2, in agreement with the model. In the model, the cloud of tidal debris close to the progenitor was stripped during the

previous pericentric passage, $\sim 800$ Myr ago, while the thinner stream was stripped during the penultimate passage, $\sim 3$ Gyr ago. Thus, the observed RR Lyrae stars were likely stripped during the most recent pericenter. A future, wider area survey around Ant 2 would be useful to search for the rest of the debris stripped during this pericentric passage and further confirm that Ant 2 is tidally disrupting.

The model predicts quite well the observed depth along the line of sight. In Figure 13, we show a histogram of the distribution of distances of the RR Lyrae stars in Ant 2, and the one from the model particles in the same footprint of our survey (the orange dots in Figure 12). The width of both distributions is strikingly similar.

## 5. AC in Ant 2

We have found eight pulsating variable stars in the footprint with magnitudes $r$ between 19.5 and 20.8, corresponding to 0.3–1.6 mag above the HB, which is the expected place for AC stars in a CMD (Catelan & Smith 2015).

There are enough observational similarities between AC and RR Lyrae stars that it is worth discussing with some detail the origin of these stars. Indeed, the first hint that led to the discovery of Ant 2 by Torrealba et al. (2019) was a group of three RR Lyrae stars in the Gaia catalog (Clementini et al. 2019) with magnitudes $G \sim 20.2$. A group of three RR Lyrae stars, very close together in the sky, with similar magnitudes,
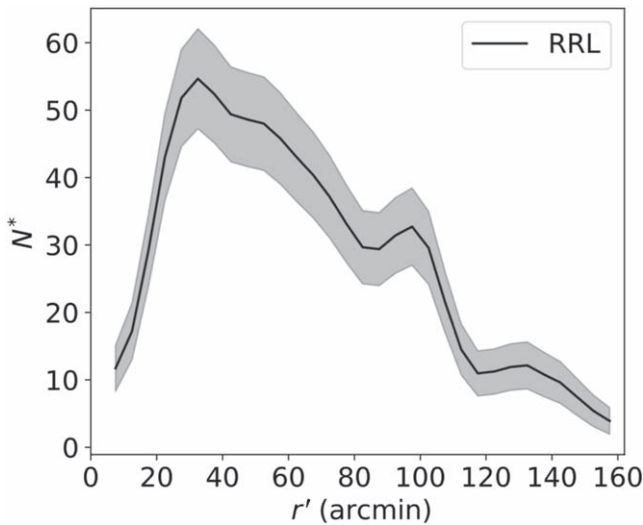
**Figure 11.** Running average of the number of RR Lyrae stars as a function of the elliptical distance ($r'$). The shaded region shows the Poisson uncertainties.
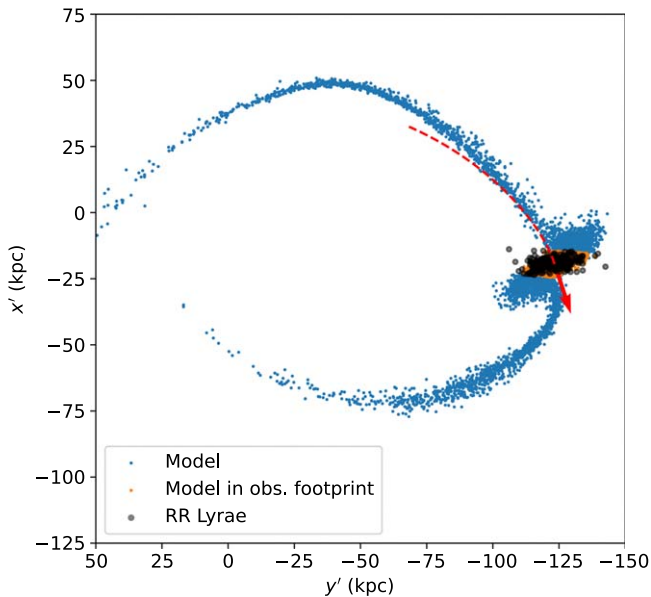


**Figure 12.** Top-down view of Ant 2 from above its orbital plane. The blue points show the stream model while the orange points show the model limited to the sky positions of the RR Lyrae stars (black circles). The model matches the observed sample of RR Lyrae. The red vector shows the present-day velocity of Ant 2, and the dotted red line shows the past orbit of Ant 2.



**Figure 13.** Distance distribution of the RR Lyrae stars in Ant 2 and the model particles within the same footprint of our survey.
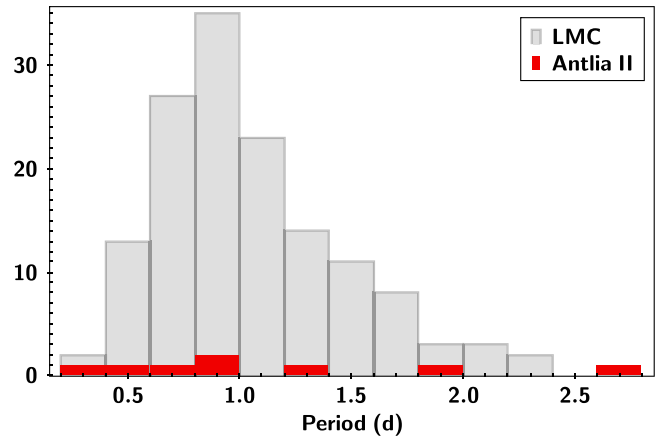


**Figure 14.** Period distribution of AC in the LMC (Soszyński et al. 2017) and Ant 2 (this work).

and similar proper motions, prompted the search for an underlying stellar population, which was indeed quickly identified. However, it was clear that the group of RR Lyrae stars was much closer than the main body of Ant 2, at distances ranging between 50 and 95 kpc. The authors speculated that the group of RR Lyrae stars may be part of material stripped out from Ant 2. In this paper, these same three RR Lyrae stars are among the group we are reclassifying as AC members of Ant 2.

The main clue that this group of stars are AC and not RR Lyrae stars is the period distribution (Figure 14). Although both types of variables have overlapping period distributions, ACs can have periods as long as ~2.5 days (Catelan & Smith 2015). RR Lyrae stars on the other hand have periods <1.0 days. In Figure 14 we show the period distribution of our sample of AC

in Ant 2 compared to that for the LMC from the Optical Gravitational Lensing Experiment (OGLE) survey (Soszyński et al. 2017). The presence of three long-period variables (>1 days) in Ant 2 fits well with the expected distribution of periods for AC found in the LMC.

AC are rare stars but they have been found in dSph galaxies around the MW, including the Magellanic Clouds (Soszyński et al. 2017), Sculptor (Martínez-Vázquez et al. 2016), Carina (Vivas & Mateo 2013; Coppola et al. 2015), Crater 2 (Vivas et al. 2020), Sextans (Mateo et al. 1995; Vivas et al. 2019), Draco (Kinemuchi et al. 2008), and also in the satellites of M31 (Martínez-Vázquez et al. 2017). It is thus not surprising that a galaxy as massive as Ant 2 will also contain a population of these variables. AC have two main formation channels. They may originate as evolved metal-poor stars of an intermediate-age population (Fiorentino & Monelli 2012, and references therein), or alternatively originate from binary evolution of old stars (e.g., Gautschy & Saio 2017). There are no obvious hints of an intermediate-age population from the CMD of Ant 2, although the large field contamination may hide such features, particularly if its overall contribution to the galaxy population is small. With the current data we cannot with certainty discard the intermediate-age formation channel for the AC.
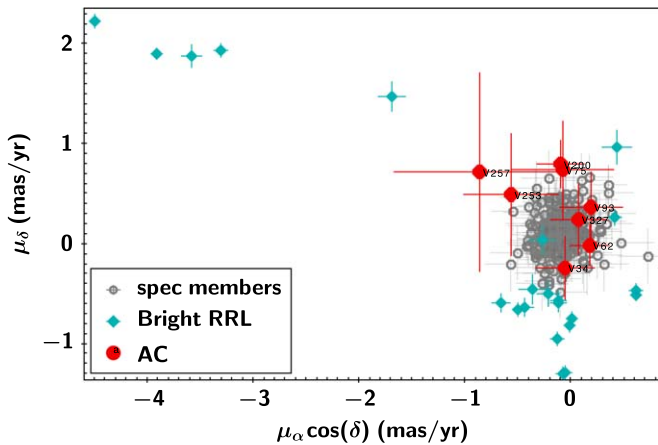
**Figure 15.** Gaia EDR3 proper motions of AC stars in Ant 2 (red circles). For reference, the plot also shows the proper motions of spectroscopic members selected by Ji et al. (2021; gray open circles), and other bright RR Lyrae in the field of Ant 2 (cyan diamonds).

A final confirmation that the group of AC are members of Ant 2 come from their proper motions. All the stars in this group are sufficiently bright to have proper motion measurements in Gaia EDR3 (Gaia Collaboration et al. 2021). In Figure 15, we show that the proper motions of all eight AC are consistent with those for stars confirmed as radial velocity members of the galaxy (Ji et al. 2021), although the errors for the faintest of our AC are quite high. In contrast, the proper motions of other bright RR Lyrae stars in the field are more widely distributed. Thus, the proper motions support this group of stars, or most of them, being members of Ant 2 rather than field halo stars. In any case, the latter is an unlikely scenario since halo RR Lyrae stars are rare at such large distances. We again estimated the expected number of RR Lyrae stars by integrating the number density radial profile of RR Lyrae from Medina et al. (2018) between 50 and 100 kpc, which resulted in 1.4 RR Lyrae stars over the full area of our survey. At most the contamination of two Galactic halo RR Lyrae stars is expected among the group of eight AC.

## 6. Conclusions

We present a variability survey of 12 deg$^2$ around the Ant 2 satellite galaxy, which reveled a large population of RR Lyrae stars (318) as well as eight AC. Ant 2 is a very large galaxy, larger than even the Small Magellanic Cloud (SMC), but with a much lower surface brightness. Additional challenges to study this galaxy are its large distance (HB at $r \sim 21.3$) and a position in the sky at low galactic latitude ($b \sim 14°$), which results in a high contamination by field stars. The large FoV of DECam was crucial to be able to survey the full galaxy over just a few days, obtaining time series with excellent signal-to-noise ratio at the level of the HB of Ant 2. The RR Lyrae stars found in Ant 2 are considered a very pure sample of members since virtually no contamination by MW RR Lyrae stars is expected at a similar distance. Based on the RR Lyrae stars we derived a distance of 124.1 kpc, with a dispersion of 5.4 kpc.

The variable star population of Ant 2 reveals some interesting facts about this galaxy:

1. Ant 2 is large. We find RR Lyrae stars over the full surveyed area. The $3\sigma$ ellipse that encloses the RR Lyrae stars has a major axis over $5°$ on the sky. Although there

is a decline on the number of RR Lyrae stars with radius, it is very likely that there will be more such stars awaiting discovery outside the observed area.

2. Ant 2 has a population of AC. First interpreted by Torrealba et al. (2019) as foreground RR Lyrae stars, we demonstrated here that it is more likely they are AC members of Ant 2. The existence of this population however does not necessarily mean that there is an intermediate-age population in the galaxy, a common interpretation when AC are present, as they also originate from evolution of binary stars in an old population. The current data does not allow us to differentiate with certainty between the formation channels.

   The previous interpretation of these stars being RR Lyrae stars was consistent with Ant 2 having lost most of its mass ($\sim 90\%$ Torrealba et al. 2019). In such scenario there would be Ant 2 tidal material in front of the main body of the galaxy. New metallicity measurements and updated proper motions indicate that although the galaxy may be disrupting, such a large mass loss is unlikely Ji et al. (2021), making the existence of debris in front of the galaxy hard to explain. The new interpretation of these stars being AC in Ant 2 solves that controversy since it does not imply there is material in front of the galaxy.

3. Ant 2 is disrupting. The spatial distribution of the RR Lyrae stars reveals an elongation ($\epsilon = 0.28$), which is approximately aligned with the reflex corrected proper motions of Ant 2 (see Ji et al. 2021, for more details). In addition, the precise distances of the RR Lyrae allow us to detect the elongation along the line of sight, which is almost perpendicular to the orbit of Ant 2. Along similar lines, there is a significant gradient in distance along the major axis of the galaxy. Based on an extensive spectroscopic survey covering a similar area to the present work, Ji et al. (2021) also detected a gradient along the major axis but for the radial velocity of RGB stars. Both gradients, distance and radial velocity, can be reproduced by a model of the disruption of Ant 2. In this model, the RR Lyrae stars we are observing here were torn apart from the main body of Ant 2 during the last pericenter passage, about 800 Myr ago.

The disruption model of Ant 2 predicts long tidal tails coming from the center of the Galaxy and extending over more than $100°$ in the sky. To search for RR Lyrae stars in the tails will be difficult with the current instrumentation because of the large search volume. However, the tidal tails of Ant 2, if they indeed exist, should be easily revealed by data from the Vera C. Rubin Observatory after 1–2 yr of survey operations.

# Appendix
# Time Series Data

Table 6 presents the individual epoch photometry in $r$ and $i$ for all the periodic variable stars measured in this work. Light curves for all the stars are provided as Figure Set 16.

**Table 6**
Time Series Photometry of Variable Stars in the FoV of Ant 2

| ID | Filter | HJD (days) | Mag (mag) | Error (mag) |
|----|--------|------------|-----------|-------------|
| V1 | $r$ | 2458472.709444 | 21.454 | 0.033 |
| V1 | $r$ | 2458472.753670 | 21.087 | 0.016 |
| V1 | $r$ | 2458472.797899 | 20.996 | 0.016 |
| V1 | $r$ | 2458472.842118 | 21.133 | 0.013 |
| V1 | $r$ | 2458504.731142 | 21.265 | 0.016 |
| V1 | $r$ | 2458504.776744 | 21.289 | 0.020 |
| V1 | $r$ | 2458504.821390 | 21.448 | 0.055 |
| V1 | $r$ | 2458504.865625 | 21.499 | 0.047 |

(This table is available in its entirety in machine-readable form.)
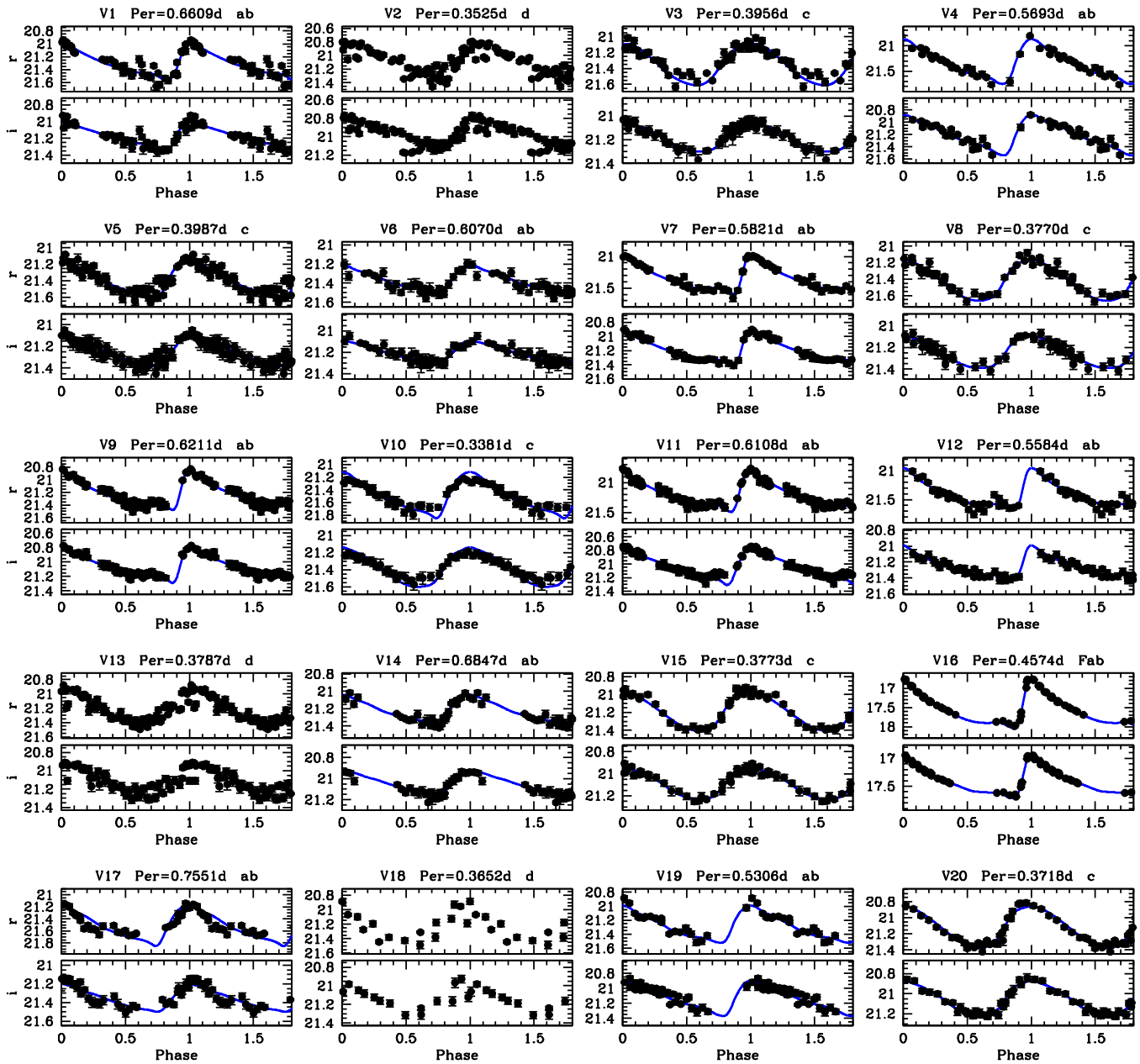
**Figure 16.** For each star the *r*, *i* data are displayed in the top/bottom panels. For all the types *ab* and *c* the underlying blue line is the best-fitted template to the light curve. The complete figure set (18 images) is available in the online journal.

(The complete figure set (18 images) is available.)

## ORCID iDs

A. Katherina Vivas ⓘ https://orcid.org/0000-0003-4341-6172
Clara E. Martínez-Vázquez ⓘ https://orcid.org/0000-0002-9144-7726
Alistair R. Walker ⓘ https://orcid.org/0000-0002-7123-8943
Vasily Belokurov ⓘ https://orcid.org/0000-0002-0038-9584
Ting S. Li ⓘ https://orcid.org/0000-0002-9110-6163
Denis Erkal ⓘ https://orcid.org/0000-0002-8448-5505

## References

Belokurov, V. 2013, NewAR, 57, 100
Besla, G., Kallivayalil, N., Hernquist, L., et al. 2007, ApJ, 668, 949
Cáceres, C., & Catelan, M. 2008, ApJS, 179, 242
Catelan, M. 2009, Ap&SS, 320, 261
Catelan, M., & Smith, H. A. 2015, Pulsating Stars (New York: Wiley)
Clementini, G., Cignoni, M., Contreras Ramos, R., et al. 2012, ApJ, 756, 108
Clementini, G., Ripepi, V., Molinaro, R., et al. 2019, A&A, 622, A60
Coppola, G., Marconi, M., Stetson, P. B., et al. 2015, ApJ, 814, 71
Dehnen, W., & Binney, J. 1998, MNRAS, 294, 429
Drake, A. J., Graham, M. J., Djorgovski, S. G., et al. 2014, ApJS, 213, 9
Drlica-Wagner, A., Bechtol, K., Mau, S., et al. 2020, ApJ, 893, 47
Erkal, D., Belokurov, V., Laporte, C. F. P., et al. 2019, MNRAS, 487, 2685
Fabrizio, M., Bono, G., Braga, V. F., et al. 2019, ApJ, 882, 169
Fiorentino, G., & Monelli, M. 2012, A&A, 540, A102
Flaugher, B., Diehl, H. T., Honscheid, K., et al. 2015, AJ, 150, 150
Gaia Collaboration, Brown, A. G. A., Vallenari, A., et al. 2021, A&A, 649, A1
Gautschy, A., & Saio, H. 2017, MNRAS, 468, 4419
Gibbons, S. L. J., Belokurov, V., & Evans, N. W. 2014, MNRAS, 445, 3788

Green, G. M. 2018, JOSS, 3, 695
Ivezić, Ž., Connelly, A. J., VanderPlas, J. T., & Gray, A. 2014, Statistics, Data Mining, and Machine Learning in Astronomy (Princeton, NJ: Princeton Univ. Press)
Ji, A. P., Koposov, S. E., Li, T. S., et al. 2021, ApJ, 921, 32
Kallivayalil, N., van der Marel, R. P., Besla, G., Anderson, J., & Alcock, C. 2013, ApJ, 764, 161
Kinemuchi, K., Harris, H. C., Smith, H. A., et al. 2008, AJ, 136, 1921
Kinman, T. D., & Brown, W. R. 2010, AJ, 139, 2014
Li, T. S., Koposov, S. E., Erkal, D., et al. 2021, ApJ, 911, 149
Martin, N. F., Ibata, R. A., Lewis, G. F., et al. 2016, ApJ, 833, 167
Martínez-Vázquez, C. E., Monelli, M., Bernard, E. J., et al. 2017, ApJ, 850, 137
Martínez-Vázquez, C. E., Stetson, P. B., Monelli, M., et al. 2016, MNRAS, 462, 4349
Mateo, M., Fischer, P., & Krzeminski, W. 1995, AJ, 110, 2166
McConnachie, A. W. 2012, AJ, 144, 4
McMillan, P. J. 2017, MNRAS, 465, 76
Medina, G. E., Muñoz, R. R., Vivas, A. K., et al. 2018, ApJ, 855, 43
Nidever, D. L., Olsen, K., Walker, A. R., et al. 2017, AJ, 154, 199
Oosterhoff, P. T. 1939, Obs, 62, 104
Pietrzyński, G., Graczyk, D., Gieren, W., et al. 2013, Natur, 495, 76
Savino, A., Koch, A., Prudil, Z., Kunder, A., & Smolec, R. 2020, A&A, 641, A96
Schlafly, E. F., & Finkbeiner, D. P. 2011, ApJ, 737, 103
Schlegel, D. J., Finkbeiner, D. P., & Davis, M. 1998, ApJ, 500, 525
Sesar, B., Ivezić, Ž., Grammer, S. H., et al. 2010, ApJ, 708, 717

Shipp, N., Drlica-Wagner, A., Balbinot, E., et al. 2018, ApJ, 862, 114
Shipp, N., Erkal, D., Drlica-Wagner, A., et al. 2021, ApJ, 923, 149
Simon, J. D. 2019, ARA&A, 57, 375
Smith, H. A. 1995, RR Lyrae Stars (CAS) (Cambridge: Cambridge Univ. Press), 27
Soszyński, I., Udalski, A., Szymański, M. K., et al. 2017, AcA, 67, 103
Stetson, P. B. 1987, PASP, 99, 191
Stetson, P. B. 1994, PASP, 106, 250
Taylor, M. B. 2005, in ASP Conf. Ser. 347, Astronomical Data Analysis Software and Systems XIV, ed. P. Shopbell, M. Britton, & R. Ebert (San Francisco, CA: ASP), 29
Torrealba, G., Belokurov, V., Koposov, S. E., et al. 2019, MNRAS, 488, 2743
Torrealba, G., Koposov, S. E., Belokurov, V., & Irwin, M. 2016, MNRAS, 459, 2370
Valdes, F., & Gruendl, R. 2014, in ASP Conf. Ser. 485, Astronomical Data Analysis Software and Systems XXIII, ed. N. Manset & P. Forshay (San Francisco, CA: ASP), 379
van der Marel, R. P., Alves, D. R., Hardy, E., & Suntzeff, N. B. 2002, AJ, 124, 2639
Vivas, A. K., Alonso-García, J., Mateo, M., Walker, A., & Howard, B. 2019, AJ, 157, 35
Vivas, A. K., & Mateo, M. 2013, AJ, 146, 141
Vivas, A. K., Olsen, K., Blum, R., et al. 2016, AJ, 151, 118
Vivas, A. K., Walker, A. R., Martínez-Vázquez, C. E., et al. 2020, MNRAS, 492, 1061
Willman, B. 2010, AdAst, 2010, 285454